Coulomb Repulsion at the Nanometer-Sized Contact: A Force Driving Superhydrophobicity, Superfluidity, Superlubricity, and Supersolidity

Chang Q. Sun,*,†,# Yi Sun,‡ Yanguang Ni,† Xi Zhang,† Jisheng Pan,‡ Xiao-Hui Wang,§ Ji Zhou,§ Long-Tu Li,§ Weitao Zheng,‖ Shansheng Yu,‖ L. K. Pan,⊥ and Zhuo Sun⊥

School of Electrical and Electronic Engineering, Nanyang Technological University, Singapore 639798, Singapore, Institute of Materials Research and Engineering, Agency for Science, Technology and Research (A*STAR), 3 Research Link, Singapore 117602, Singapore, State Key Lab of New Ceramics and Fine Processing, Department of Materials Science and Engineering, Tsinghua University, Beijing, 100084, China, Department of Materials Science, Jilin University, Changchun 130012, China, Engineering Research Center for Nanophotonics and Advanced Instrument, Ministry of Education, Department of Physics, East China Normal University, Shanghai 200062, China, and School of Physical Science and the Key Laboratory of Low-Dimensional Materials and Application Technologies (Ministry of Education), Xiangtan University, Hunan 411105, China

Superhydrophobicity, superfluidity, superlubricity, and supersolidity (4S) at the nanometer-sized liquid−solid or solid−solid contacting interfaces have long been issues of puzzling with the common characteristics of nonsticky and frictionless motion. Although the 4S occurrences have been extensively investigated, the mechanism behind the common characteristics remains unclear. From the perspectives of broken-bond-induced local strain and the skin-depth charge and energy quantum trapping and the associated nonbonding electron polarization, we proposed herewith that the Coulomb repulsion between the "electric monopoles or dipoles locked in the elastic solid skins or the solidlike covering sheets of liquid droplets" forms the key to the 4S. The localized energy densification makes the skin stiffer and the densely and tightly trapped bonding charges polarize nonbonding electrons, if exist, to form locked skin monopoles. In addition, the sp-orbit hybridization of F, O, N, or C upon reacting with solid atoms generates nonbonding lone pairs or unpaired edge electrons that induce dipoles directing into the open end of a surface. The monopoles and dipoles can be, however, demolished by UV radiation, thermal excitation, or excessively applied compression due to ionization or sp orbit dehybridization. Such a Coulomb repulsion between the negatively charged skins of the contacting objects not only lowers the effective contacting force and hence the friction but also prevents charge from being exchanged between the counterparts of the contact. Being similar to magnetic levitation, such Coulomb repulsion should be the force driving the 4S. Density function theory calculations, X-ray photoelectron spectroscopy, scanning tunneling microscopy/spectroscopy, and very low energy electron diffraction measurements have been conducted to verify the proposal. In particular, agreement between theory predictions and the measured size dependence of the elastic modulus, lattice strain, core−electron binding energy shift, and band gap expansion of nanostructures evidence the validity of the proposal of interface Coulomb repulsion.

1. Introduction

Superhydrophobicity, superfluidity, superlubricity, and supersolidity (4S) at the nanometer-sized liquid−solid or solid−solid contacting interfaces are indeed fascinating, which have continued stimulating interest of study for decades. The 4S phenomena that share the common characteristics of chemically nonsticky and mechanically frictionless motion are of great importance not only to practical applications but also to fundamental understanding of interactions between the nanometer-sized contacts. Unfortunately, the underlying mechanism remains unclear despite various modeling theories in terms of surface energies[1] or the geometric roughness[2] for certain occurrences such as a water droplet resting on the repellent lotus leaf[3] and a water strider standing on the water surface.[4,5] From the perspectives of chemical bonding and the unusually electronic and energetic configurations in the surface of skin depth, we proposed in this work that the Coulomb repulsion between the "electric monopoles or dipoles locked in the elastic solid skins or the solid-like elastic liquid skins" forms the key to the 4S. This article is arranged as follows. In the next overview section, we will summarize the observations, the current understandings and the fundamental challenges regarding the 4S. In Section 3, we will introduce the bond order-length-strength (BOLS) correlation theory[6] and its derivatives on the tightly trapped charge and energy in the surface skin. We will also discuss the formation of surface monopoles due to the polarization of nonbonding unpaired electrons by the surface quantum trapping. We also introduce the formation of surface dipoles due to C, O, N, F addition as well as the annihilation of these dipoles and monopoles by UV radiation or thermal excitation, based on our previous understandings.[6−8] In section 4, we will show our predictions and verification of the curvature dependence of the skin charge density, energy density, and the quantum trap depth. In order to verify the predictions specifi-

* To whom correspondence should be addressed. E-mail: ecqsun@ntu.edu.sg.
† Nanyang Technological University.
# Xiangtan University.
‡ Agency for Science, Technology and Research (A*STAR).
§ Tsinghua University.
‖ Jilin University.
⊥ East China Normal University.

cally, we will show the quantitative consistency between predictions and measurements of the size-induced lattice strain, elastic modulus, core level shift and band gap expansion of nanostructures of various materials. We are doing so because the lattice strain corresponds to charge density (the total number of charge reserves but the sample volume shrinks) and the elastic modulus to the energy density. The core level shift and band gap expansion correspond to the potential trap depth. The size dependence has been shown to be dominated by the few-atomic layers in the surface skin. Besides, we will show the following: (i) the density functional theory (DFT) calculation results of the width dependence of the densification of the trapped and polarized density-of-states (DOS) and the densification of charge of graphene nanoribbon; (ii) charge polarization of cuboctahedral (CO) gold nanoclusters of 13, 55, 147 atoms. The calculated results coincide excitingly with the latest scanning tunneling microscopy/spectroscopy (STM/S) observations of gold chain end states,[9] thickness dependence of the near Fermi energy local states gold nanowires,[10] and Ag monomer and dimer,[11] as well as the shell-resolved bond contraction of Au cluster.[12] We also conducted a X-ray photoelectron spectroscopy (XPS) study of the evolution of roughened SrTiO surface with trapped and polarized valence DOS and core level shift and present a summary of previous STM/S and very-low-energy electron diffraction (VLEED) investigations of oxygen adsorbed Cu(001) surface with demonstration of the presence of the nonbonding lone pairs, the dipoles, and the associated energy states. Confirmation of theoretical expectations evidence the validity of the proposed mechanism and the ways of our thinking and approaching about the fascinating 4S occurrences.

2. Overview: Historical challenge

2.1. Surface Superhydrophobicity and Superhydrophilicity Transition. Superhydrophobic materials have surfaces that are extremely difficult to wet with water contact angles in excess of 150° or even greater. In the past decade, surfaces with ultrahydrophobicity have aroused much research interest with their potential applications in self-cleaning coatings, microfluidics, biocompatible materials, and so on. Many physical chemical processes, such as adsorption, lubrication, adhesion, dispersion, friction, and so forth, are closely related to the wettability of materials surfaces.[13,14] Examples of hydrophobic molecules include alkanes, oils, fats, wax, and greasy and organic substances with C, N, O, or F as the key constituent element.

Many of these superhydrophobic materials found in nature display characteristics fulfilling Cassie's law[2] stating that the surface contact angle can be increased by simply roughing up the surface, that is, the surface roughness and the contact area are suggested to be the factors of dominance. For instance, fluids can slip frictionlessly past pockets of air between textured surfaces with micrometer-scale grooves or posts of tiny distances.[15] The slip length for water is almost ten times longer than previously achieved, indicating that engineered surfaces can significantly reduce drag in fluid systems. On the basis of Cassie's law and thermodynamics considerations, Fang et al.[16] and Li et al.[17] designed tunable superhydrophobic surfaces to control the directional motion of water droplets by varying the pillar width and spacing simultaneously. Varying the gradient of the stiffness of a microbeam could also drive directional movement of liquid droplets on a microbeam.[18]

An experiment[4] showed that a water strider statically standing on water can bear a load up to 60 times its body weight with its middle and hind legs, which tread deep puddles without piercing the water surface. This fact has been ascribed as the superhydrophobicity of the water strider legs due to "bio-wax" coatings. Another comparative experiment[5] using the real water strider legs and artificial legs made of wax-coated steel wires revealed that the adaptive-deformation capacity of the real leg through its three joints makes a more important contribution to the superior load-bearing ability than the superhydrophobicity.

What is even more amazing is that the hydrophobic surface can switch reversibly between superhydrophobicity and superhydrophilicity when the solid surface is subject to UV radiation[19] which creates electron−hole pairs.[20] After being stored in the dark over an extended period, the hydrophilicity is once again lost.

2.2. Superfluidity in Nanochannels. The transport of fluid in and around nanometer-sized objects with at least one characteristic dimension below 100 nm enables the superfluidic occurrences that are impossible on bigger length scales.[21] Nanofluids have significantly greater thermal and mass conductivity in nanochannels compared with their base fluids.[22] The difference between the nanofluid and the base fluid is the high value of surface-to-volume ratio that increases with the miniaturization of the dimensions of both the fluid and the channel cavity in which the fluid is flowing. This high flowing rate of nanofluids in nanochannels will result in the surface-charge-governed transport for cell separation applications.[21]

On the other hand, the rate of the pressure-driven water flow through carbon nanotubes (CNTs) is orders higher than predictions by conventional fluid-flow theory.[23] The thinner the channel cavity is, the faster the fluid-flow rate will be under the same pressure.[24] This high fluid velocity results from an almost frictionless interface between the CNT wall and the fluid droplets.[25] A molecular dynamics calculation[26] suggested that water flow in CNT could generate a constant voltage difference of several millivolts between the two ends of a CNT due to interactions between the water dipole chains and charge carriers in the CNT, which might also contribute to the abnormal frictionless fluid flow in the CNT.

The superfluidity is generally described by an electro-kinetic theory of the electrical double layer (EDL) scheme.[27] The EDL channel can be operated as field-effect transistors to detect chemical and biological species label-free, while transport through nanochannels leads to analyte separation and new phenomena when the EDL thickness becomes comparable to the smallest channel opening.

2.3. Superlubricity in Dry Sliding. More fascinating observations include the ultralow-friction linear bearing of CNTs and the superlubricity at dry nanocontacts sliding in high vacuum.[28,29] It has been observed using transition electron microscopy that the inner walls of a multiwalled CNT can slide back and forth with respect to the outer walls of the CNT, being free from wear for all cycles of motion.[30] Surface energy calculations suggested that the force retracting the core nanotubes back into the outer tubes was 9 nN, being much lower than the van der Waals forces pulling the core nanotubes back into their sheath. The removal of the outer walls of the CNT was attributed to the highly localized dissipation at defect scattering sites, located primarily at the ends of the tube. The demonstration of ultralow friction between multiwalled CNT layers is a valuable confirmation that they will be useful mechanical components in molecular nanotechnology such as molecular bearing.

The occurrence of quantum friction is a kinetic process of energy dissipation (with energy $E = f_r s$ with f_r being the friction force and s the sliding distance) due to the phonon (heat) and

Coulomb Repulsion at the Nanometer-Sized Contact

J. Phys. Chem. C, Vol. 113, No. 46, 2009 **20011**

electron excitation (electron−hole pair production) during sliding.[31] A state of ultralow friction is reached when a sharp tip slides over a flat surface and the applied pressure is below a certain threshold, whose value is dependent on the surface potential sensed by the tip and the stiffness of the contacting materials.[26,32,33]

A comparative study of hydrogen- and deuterium-terminated single-crystal diamond and silicon surfaces revealed that the hydrogenated surface (terminated with H^+) exhibited higher friction than the surface passivated with $^2H^+$. The additional neutron in the $^2H^+$ should play a certain yet unclear role of significance because of the possible adsorbate size difference.[31] A remarkable dependence of the friction force on carrier type and concentration has been discovered by Park et al.[34] on doped silicon substrates. An experiment of a biased conductive TiN coated tip of an atomic force microscope sliding on a Si substrate with patterned p and n stripes revealed that charge depletion or accumulation results in substantial differences in the friction force. A positive bias applied to the p-region causes a substantial increase of the friction force compared to the n region because of an accumulation of holes (+ charged) in the p region. No notable variation of friction force was observed between n and p regions at negative bias. Both observations[31,34] indicate clearly that the positively charged (H^+) tip or substrate (electronic holes +) would induce high friction force.

The superlubricity phenomenon was explained using the classical Prandtl−Tomlinson (PT) model[35,36] and its extensions, including thermal activation, temporal and spatial variations of the surface corrugation, and multiple-contact effects.[32] Most recent progress suggests that the friction force depends linearly on the number of atoms that interact chemically across the contact.[37] According to the one-dimensional PT model, the slider atoms feel the periodic potential of the substrate surface atoms as they slide over them, experiencing a net force that is the sum of individual instantaneous friction force on each atom resulting from the gradient of the periodic potential.

2.4. Supersolidity of ^4He: Superelasticity and Superfluidity. At temperature below 200 mK,[38] Helium 4 (^4He) crystal is readily decoupled into fragments in a torsional oscillator to exhibit superfluidic nature, that is, frictionless motion without viscosity;[39,40] meanwhile, the ^4He crystal fragments are stiffer than expected and hence react elastically to a shear stress.[41] The individual segment of the ^4He crystal would be thus both superelastic and superfluidic in motion.

The superfluidity of ^4He solid is usually described in terms of Bose−Einstein condensation or quantum statistics in energy space. All particles occupy the lowest energy states simultaneously. A scenario in real space is lacking though the crystal defect has recently been recognized as the key to the supersolidity.[42] The quantum defects such as atomic vacancies are of the order of one nanometer in size or thereabouts[43] and the supersolidity is related to structural disorders[44] such as dislocations, vacancies, grain boundaries, or ill-crystallized regions where the under-coordinated atoms dominate. According to Pollet et al.,[43] inside a dislocation or a grain boundary the local stress is anisotropic and sufficient to bring the vacancy energy to zero to follow the law of Bose−Einstein condensation, so that the defect is invaded by vacancies that are mobile and superfluidic. Solid ^4He could contain a network of defects and if these defects were connected to each other, mass could flow from one side of the crystal to the other without friction during the torsional oscillation.

Understanding the observations of nonlinear rotational susceptibility in samples of solid helium below temperatures of 200 mK has been a subject of controversy. According to Anderson,[42] the observations are conjectured to be describable in terms of a rarified Gross−Pitaevskii superfluid of vacancies with a transition temperature of about 50 mK, whose density is locally enhanced by crystal imperfections. The observations can be greatly affected by this density enhancement. Therefore, disorder and defects that could enhance the local density appear to play an important yet uncertain role in the supersolidity of ^4He crystals.[45]

2.5. Challenges and Objective. The 4S occurrences result from the reduction of friction force ($f_r = \mu N$ with μ being the friction coefficient and N the contacting force). The lowering of the f_r will reduce the process of friction or the extent of phonon and electron excitation. Although the 4S has been extensively investigated and widely applied, the common law governing the 4S remains unknown. One surprising fact is that these 4S effects share a general identity of nonsticky and frictionless motion-with lowered effective contacting pressure and reduced friction coefficient. The 4S phenomena must share a common elastic and repulsive origin for the nonsticky and low-friction in addition to the energetic and geometric descriptions of the existing models. Considerations from the perspectives of surface roughness and surface energy seem insufficient because the chemistry and the charge identities do alter at the surface skin up to two interatomic spacings.[46] In particular, the hydrophobicity−hydrophilicity recycling effect caused by UV irradiation and the subsequent dark aging is beyond the scope of Cassie's law and the PT mechanism of air pockets dominance. Furthermore, the superhydrophobicity of alkanes, oils, fats, wax, and the greasy and organic substances is independent of the surface roughness. Although the crystal defects have been recognized as the key to the supersolidity of ^4He solid, correlation between the defects and the superelasticity and superfluidity is yet to be established. Therefore, a deeper insight into the chemical nature of the surfaces is necessary for one to gain a better understanding of the origin for the 4S.

The objective of this contribution is to show the essentiality of considering the 4S phenomena, as a whole, from the perspective of the chemical nature of the surface. In addition to the artificially structural configurations, the chemical bonding and the associated surface energy and charge densification as well as the charge polarization of under-coordinated atoms in the surface region play a role of dominance in the 4S. This perspective allows us to clarify, for the first time, that the interfacial Coulomb repulsion between the "electronic monopoles or dipoles locked in the stiffened solid skins or the solid-like liquid skins" governs the 4S occurrences.

3. Principles

3.1. Broken-Bond-Induced Local Strain and Skin-Depth Charge and Energy Quantum Trapping. According to the bond-order-length-strength (BOLS) correlation theory,[6,47] bonds between under-coordinated atoms at sites surrounding structural defects, disorders, dislocations, atomic vacancies, terrace edges, grain boundaries, and at the surfaces, become shorter and stronger in comparison to those between fully coordinated atoms in the bulk interior. The bond order deficiency-induced bond contraction has happened globally to surfaces of solid[12,46] and liquid,[48,49] dimers,[50,51] atomic chains,[52−54] carbon nanotubes,[55] graphene ribbons,[56] terrace edges,[57,58] nanograins,[12,59,60] and the negatively curved surfaces of nanocavities.[61] The spontaneous process of bond contraction is associated with bond energy gain or potential trap depression. As a result, localized densification of charge and energy takes place in the surface of skin depth.[12,46]

The energy densification enhances the local elasticity (the bulk modulus is proportional to the energy density[62]) or stiffness (the product of the skin thickness and the elastic modulus) of the skin and the densely and tightly trapped charges will polarize existing surface nonbonding electrons such as those in the half-filled s-orbital of gold or the π-electrons of sp^2 hybridized carbon. The localized polarization of the surface nonbonding s-electrons makes $Au(4f^{14}5d^{10}6s^1)$, $Ru(4d^75s^1)$, $Rh(4d^85s^1)$, and $Ag(4d^{10} 5s^1)$ nanocrystals to be nonconductive and magnetic[63] because the otherwise conducting electrons turn to be the tightly locked monopoles. As a result of the potential trap depression, the gap between the conduction and the valence band of a semiconductor will expand[64] and the core-level binding energy of a specimen will shift positively to deeper energies, which has been observed frequently.[6,46,47] For instances, the first layer spacing of Nb(001) surface contracts by 12% associated with a 0.50 eV positive shift of its $3d_{3/2}$ binding energy.[65] A $(10 \pm 3)\%$ contraction of the first layer spacing of Ta(001) has caused its $4f_{5/2(7/2)}$ level to shift by 0.75 eV with a local charge densification.[66] Atomic layer-resolved 2p level positive shift of Ni surface has been detected by Matsui et al.,[46] and the co-ordination-resolved C 1s level shift of the few-layer graphene has also been probed by Kim et al.[67] and Hibino et al.[68] The band gap of Si nanowires expands from 1.1 to 3.5 eV when the wire diameter is decreased from 7 to 1.3 nm associated with a 10% Si−Si spacing contraction.[64]

Within skin depth of the surface, the curvature K^{-1} (K being the dimensionless form of size is the number of atoms lined along the radius of a spherical dot) dependence of the effective atomic coordination (z_i), bond length (d_i), charge density (n_i), energy density (elastic modulus, B_i), and the potential trap depth (E_i) in the ith atomic site follow the relations[6]

$$
\begin{cases}
z_1 = 4(1 - 0.75K^{-1}); & \text{(effective coordination)} \\
z_2 = z_1 + 2; \; z_3 = 12 \\
d_i = C_i d_b = 2d_b[1 + & \text{(bond contraction coefficient)} \\
\exp((12 - z_i)/(8z_i))]^{-1} \\
n_i = n_b C_i^{-3} & \text{(charge density)} \\
B_i = B_b C_i^{-(m+3)} & \text{(bulk modulus)} \\
E_i = E_b C_i^{-m} & \text{(potential trap depth)}
\end{cases}
$$
(1)

The m is the bond nature indicator; for metals and compounds, m has been optimized to be approximately one and four, respectively. The subscript i denotes the ith atomic layer counted from the outermost to the center of the specimen and the subscript b denotes the corresponding bulk values. Therefore, we can focus on the energetic and electronic behavior of skins while keeping in mind that the core interior ($i > 3$) of a nanostructure remains as is in the bulk.[12,46] Figure 1 shows the coordination-resolved bond length contraction coefficient in comparison with the measured data for atomic chains, liquid and solid surfaces, Au nanoparticles, graphite and CNT, as discussed above and in the context of ref 6.

3.2. Curvature-Resolved Charge and Energy Densification, and Potential Trap Depression. Given the Lennard-Jones potential, $u(r)$, for instance, and taking the atomic distance r and the equilibrium bond length d, the bulk modulus B and stress P (hardness) can be derived as

$$
B = -V\frac{\partial P}{\partial V}\Big|_{r=d} = -V\frac{\partial P}{\partial r}\frac{dr}{dV} =
$$
$$
-V\frac{\partial}{\partial r}\left(-\frac{\partial u(r)}{\partial r}\frac{dr}{dV}\right)\frac{dr}{dV} \propto \frac{E_b(d)}{d^3}
$$
$$
P = -\frac{\partial u(r)}{\partial V}\Big|_{r \neq d} =
$$
$$
-\frac{\partial u(r)}{\partial r}\frac{dr}{dV} \propto \frac{E_b(r)}{r^3}
$$
(2)

where $E_b(d)$ is the equilibrium bond energy and $P = -\partial u(r)/\partial V|_{r \neq d}$ is the pressure. At equilibrium, $P = 0$. The Young's modulus, Y, is related to the bulk modulus B by $Y \sim 3B$ if the Poisson ratio is negligible. It is ready to show that the hardness at the ith atomic site is also proportional to energy density though the hardness corresponds to $P = -\partial u(r)/\partial V$ at nonequilibrium site. Equation 2 indicates that the local elastic modulus and the hardness depend intrinsically on the energy density at the atomic site under, respectively, the equilibrium and the nonequilibrium ($r \neq d$) conditions.

The spontaneous lattice strain and bond energy gain will enhance the surface elasticity by $\Delta B_i/B_b = C_i^{-(m+3)} - 1 > 0$, charge density by $\Delta n_i/n_b = C_i^{-3} - 1 > 0$, and the potential well depth by $\Delta E_i/E_b = C_i^{-m} - 1 > 0$. If taking $z_1 = 4$ and $m = 4$ for a flat compound surface, $C_1 = 0.88$, the B_1 in the first atomic spacing is $B_1/B_b = 0.88^{-7}$, which is $\sim$2.5 times that of the bulk. Similarly, the charge density is $n_i/n_b = C_i^{-3} = 0.88^{-3} = 1.47$ times that of the bulk. The potential well trap depth is $E_i/E_b = C_i^{-m} = 1.14$ for $m = 1$ and 1.67 for $m = 4$ times the original depth.

By using nanoindentation, one can readily measure the surface hardness to gain information about the surface energy density. The hardness of the TiCrN surface skin was measured to be twice that of the bulk interior, evidencing the broken-bond-enhanced surface energy density.[69] Similar results have been frequently reported as summarized in refs 6 and 70.

3.3. Size Dependence of the Lattice Strain, Energy Density and the Potential Trap Depth of Nanostructures. Generally, the size dependence of a detectable quantity, $Q(K)$, can be described as[70]

$$
Q(K) = Q(\infty)\Big[1 + \sum_{i \leq 3}\gamma_i(q_i/q_0 - 1)\Big] = Q(\infty)[1 + \Delta_q]
$$
(3)

$Q(\infty)$ is the bulk constant and γ_i is the surface-to-volume ratio. The quantity of q_i/q_0 is the ratio of the density of Q at the ith atomic site to that in the bulk interior. The Δ_q is the surface-induced perturbation to Q. Equation 3 indicates that the q_i/q_0 defines the origins while the γ_i determines the extent of change. The γ_i value depends on the shape, size, and curvature (K, τ, K^{-1}) of a specimen. Equation 3 indicates that the charge density, energy density, potential trap depth of a nanostructure is strongly correlated through the order, nature, length, and energy (z, m, d_i, E_i) of bonds in the surface skin up to three atomic layers in depth. If $q_i/q_0 = 1$ (or $C_i = 1$), none of the charge density, energy density, potential trap depth at the ith atomic site will change. Taking a sphere with radius R as a sample, the surface-to-volume ratio can be derived for the first atomic shell of d_i thick

Coulomb Repulsion at the Nanometer-Sized Contact

J. Phys. Chem. C, Vol. 113, No. 46, 2009 **20013**

$$\gamma_i = d(\ln V) = \frac{\int_{v_1}^{V} dV}{V} = \frac{4\pi \int_{R-d_i}^{R} R^2 dR}{4\pi R^3/3} =$$

$$1 - \left(\frac{R-d_i}{R}\right)^3 \cong \frac{3C_i}{K} \quad (4)$$

where K is the number of atoms lined along the radius of the nanosphere or across the thickness of a thin film or the wall thickness of a nanotubes. If all bonds in the nanocrystal contribute to the size effect, the integral over the size of $R = 0$ to R, eq 4 becomes unity. Therefore, the measured K^{-1} dependence of these quantities indicates clearly the dominance of the strained bonds in the surface shell of limited thickness in determining the size-induced change. Hence, the broken-bond-induced local strain and the skin-depth charge and energy quantum trapping in the outermost three atomic layers[12,46] are the key to the observed size dependence while bonds between the fully coordinated atoms in the core interior remain as they are in the bulk.

3.4. Formation and Annihilation of Surface Monopoles and Dipoles.

3.4.1. Surface Monopole Formation: Polarization of Nonbonding Electrons. As a consequence of the skin-depth strain and charge and energy quantum trapping, the densely trapped bonding charges in deeper energy levels will polarize the nonbonding unpaired electrons with energy in the upper edge of the conduction band, such as the nonbonding unpaired π-electrons of alkanes and graphite or the otherwise conducting electrons in the half-filled outermost s-orbital of metals such as Au, Ag, Rh, and Ru. These nonbonding electrons are usually delocalized and they dominate the electrical and thermal conductivity of the bulk materials. However, near the broken bonds at the surface, these electrons will be polarized by the tightly trapped bonding electrons to form the locally locked monopoles, so that they make no longer contributions to the conductivity, which leads to the conductor−insulator transition of nanostructured noble metals.[71] On the other hand, the densely trapped and polarized electrons form electric monopoles at the edges, which present themselves as defect states,[72] chain end states,[9,73] terrace edge states,[74,75] and surface states.[57] The polarization of nonbonding charges by the trapped bonding electrons also split the conduction band into two branches in ultrathin films or nanostructures, as observed in the cases of Au, Ag, Pb, and so forth.[76−79] The artificial band gap width increases with the inverse of cluster size.

The sp^2 orbit hybridization of carbon in graphene, graphite, and CNT generates three σ-bond and one nonbonding π-electron for each carbon atom. Bond contraction in the CNT and the
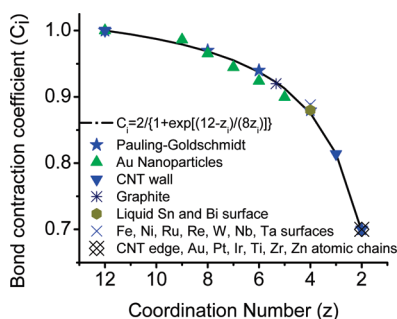

Figure 1. Atomic CN-resolved bond length contraction coefficient in comparison with measured data from atomic chains, liquid and solid surfaces, Au nanoparticles, graphite, and CNT; see the context discussion and ref 6.

graphene sheet causes charge and energy densification as well, and in particular at edges with the polarization of the π-electrons emerging as the edge states.[55,56]

However, for the intrinsic and p-type semiconductors, no monopole could form at the surface because of the lacking of the excessive nonbonding electrons though the skin-depth quantum trapping remains, as confirmed by Park et al.[34]

3.4.2. Surface Dipole Formation. The hybridization of sp orbits of the electronegative atoms such as N, O, and F produces four directional orbits, each capable of being occupied by two electrons, forming a tetrahedron, like NH_3, H_2O, and HF molecules. These four directional orbits can hence support the occupancy of eight electrons.[7] The O atom, for example, has six electrons and requires another two electrons to complete its valence shell. Therefore, the O forms two bonds with the nearest neighboring atoms by catching one electron from each of its two neighbors to share the orbits, while its remaining two orbits are occupied by the lone pair electrons of the O. Similarly, the sp orbit hybridization of N and F is associated with one and three lone pairs, respectively. These lone pairs polarize nearby atoms, causing their change to be locally locked dipoles directing into the open end of a surface, in most cases.

The presence and locking of the monopoles or dipoles determine many intriguing properties of nanostructures, such as the magnetic and insulating noble metal clusters,[63,80] diluted magnetizm in oxides,[81] and the edge states in graphene ribbons,[56] in addition to the discussed 4S. More evidence for O and N induced nonbonding lone pairs and the associated surface dipoles generation and annihilation by annealing have been extensively addressed in refs.[7,8]

3.4.3. Surface Charge Depletion. The UV radiation with excitation energy around 3.0 eV could break chemical bonds and ionize surface atoms, which could turn the hydrophobic surface to be hydrophilic, as it has widely been observed. Ar^+ sputtering the surface is expected to have the same function of removing dipole or monopole temporarily. If the polarized electrons are removed by UV irradiation, sputtering, or thermal excitation, the 4S characteristics would be lost. Aging of the specimen will recover the surface charges. The effect of UV radiation reversing effect is the same as that observed in the surface magnetizm of noble metal clusters and the dilute magnetizm of oxide nanostructures.[63,80,81] Experimental investigations[7] revealed that thermal annealing at temperatures of 600 K or above, oxygen orbital dehybridization takes place and the lone pair-induced Cu surface dipoles vanish. However, aging the samples in the ambient will recover the sp-hybridization and the dipoles as well. It is expected that surface bias to a certain extent may also cause the depletion of the locked charges though this expectation is subject to verification. Overloaded pressure in the dry sliding will overcome the Coulomb repulsion, as the energy dissipation by phonon and electron excitation could occur under the applied pressure. On the other hand, with a sufficiently large difference in the electroaffinity between the contact media, a chemical bond may form under certain conditions such as heating, pressure, or electric field, and the interface will be adherent.

One point that needs to be noted is that the common property of the nonbonding states is their extremely low interaction energy of only about 10^{-2} eV compared to the bond energy of $2-8$ eV for ionic or covalent bonds.[7] The nonbonding interactions contribute insignificantly to the Hamiltonian and hence can hardly be calculated using quantum mechanics approaches.[56] Another pronounced characteristic exhibited by nonbonding electrons are their strongly localized and inhomogeneous nature.
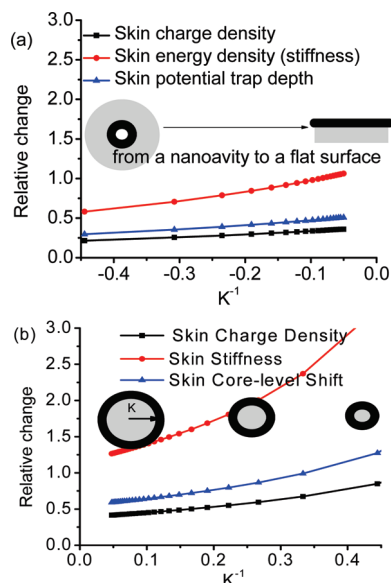
Figure 2. (a) Theoretically predicted curvature (K^{-1}) dependence of the skin charge density, energy density (elasticity), and potential trap depth (core level shift) of a specimen changing from bulk interior ($K^{-1} \sim -\infty$, not shown), nanocavity ($K^{-1} < 0$), flat surface ($K^{-1} = 0$), spherical dot ($K^{-1} > 0$) to a cluster of a few atoms ($K^{-1} \sim \infty$).

Despite their insignificant contribution to the total energy, or the Hamiltonian, of the entire solid, these nonbonding electrons add, however, DOS to the forbidden bands or to the tails of the conduction and valence band of semiconductors, forming impurity states.[82]

4. Results and Discussion

4.1. BOLS Prediction and Verification.

4.1.1. Curvature Dependence of the Skin Charge Density, Energy Density, and Potential Trap Depth. The BOLS predicted that within the skin-depth, local strain and charge and energy quantum trapping occurs. The extent of strain or densification and the quantum trapping is curvature dependent because of the curvature dependence of the effective atomic coordination,[70] $z_1 = 4(1 - 0.75/K)$; $z_2 = z_1 + 2$ and $z_3 = 12$. In order to verify the predictions specifically, we first calculated the curvature dependence of the skin charge density, energy density, and potential trap depth averaged over the outermost three atomic shells using eq 1. For the lattice strain, $q_i/q_0 = C_i$; for the elastic modulus, $q_i/q_0 = C_i^{-(m+3)}$; for the band gap expansion or the core level shift, $q_i/q_0 = C_i^{-m}$. The m value was taken as 4 for compounds and organic specimens, including water.[6] $K^{-1} = 0$, < 0, and > 0 represent, respectively, a flat surface, the inner surface of a microchannel cavity, and the outermost surface layers of a spherical dot. Results shown in Figure 2 indicate that the potential trap depth, the energy and charge density in the surface region are always higher than those in the bulk interior ($K^{-1} \sim -\infty$), and these quantities increase with the specimen's curvature.

Predictions agree with the recent findings that the surface charge density is directly proportional to the inverse of the drop size.[83] As the particle diameter drops to below 10 nm there is considerable increase in the surface charge density as compared with the limiting values seen for particles larger than 20 nm. A substantial charge transfer from the core interior of Ag clusters to the 5s and 4d orbits of surface Ag atoms has been obtained in the density functional theory (DFT) calculations.[84] A DFT calculation[85] also revealed that Au atomic rows deposited on

TiO$_2$ surface are negatively charged with about 1.1 electron charge compared to the free-standing structures. Thermally reshaping of gold aerosol particles in the 20 nm range has led to the high degree of crystallinity and monopolar charging behavior.[86] The particles are charged singly, doubly, triply, etc., depending on the annealing temperature or the crystallinity. Nasibulin et al.[87] also measured the negative charging of the structurally ordered CNTs and maghemite (γ-Fe$_2$O$_3$) particles. CNTs form spontaneously charged bundles carrying up to five elementary electrical charges. Leung et al.[88] measured the electrostatic surface potential of individual DNA and avidin molecules using Kelvin probe force microscopy and atomic force microscopy and found the surface negative (or positive) charging of biomolecules. These observations provide evidence for the predicted surface charging effect not only to gold, CNT, and oxide, but also organic specimens.

Most strikingly, a recent X-ray reflectivity measurement of liquid Bi, Sn, Ga, In, and K surfaces[48,49] revealed that the liquid is indeed capped with a strained layer of atoms of a charge density higher than that of their bulk solid. The spacing between the first and second layers of Sn contracts by 10%.[49] Jakubczyk et al.[89] investigated the surface pressure evolution of the droplet radius of aqueous suspension of nanospheres. The thermodynamic states of the surface layer formed of nanospheres have been identified to be composed of the surface gas, surface gas−liquid coexistence, surface liquid, and surface solid. Therefore, the liquid droplet is indeed capped with a solidlike and elastic skin with tightly trapped charges due to the universal surface bond contraction and quantum trapping. These discoveries are consistent with the BOLS expectation of the broken-bond-induced local strain and skin-depth quantum trapping of charge and energy. A recent experimental work[90] revealed that the surface charges of confined water can induce a strong surface field that promotes the forming of thicker water lubrication film on oxide. All the observations provide firm evidence for the surface charge and energy quantum trapping.

4.1.2. Size Dependency of Charge Density, Energy Density, and Trap Depth. In order to further verify quantitatively the theoretical predictions of skin-depth quantum trapping of charge and energy and the potential trap depression, we averaged the lattice strain, elastic modulus, core-level shift, and band gap expansion of nanostructures over the entire specimen and compared them with experimental results. In using eq 2, we took the given $z_1 = 4(1 - 0.75/K)$, and $z_2 = z_1 + 2$ relations, and the previously optimized values of $m = 1$ and 4 for metals and ZnO, respectively. A core−shell configuration is used. Generally, the surface-to-volume ratio $\gamma_i = \tau C_i/K$ with $\tau = 3$, 2, and 1 representing the dimensionality of a spherical dot, a cylindrical rod, and a thin slab, respectively.

Figure 3 shows the consistency between theoretical expectations and the measured size dependence of the lattice strain of Cu nanostructures,[91−93] the elastic modulus of ZnO nanowires,[94] the core level shift of Cu and Pd nanostructures,[71,95] and the band gap expansion of Si nanowires.[64,96,97] It is seen from the matching that the binding energy shifts further by 45% for Cu and Pd nanostructures[6] compared to the bulk values. The band gap of Si expanded by up to 200% when the Si diameter approaches 1.3 nm.[64] These findings indicate that the potential trap is indeed deepened and the extent of depression depends on the sample size and the nature (m value) of the bond involved. The elastic modulus or the energy density is enhanced by 60% at the smallest size of ZnO. The consistency between predictions and observations provides sufficient evidence for the proposals
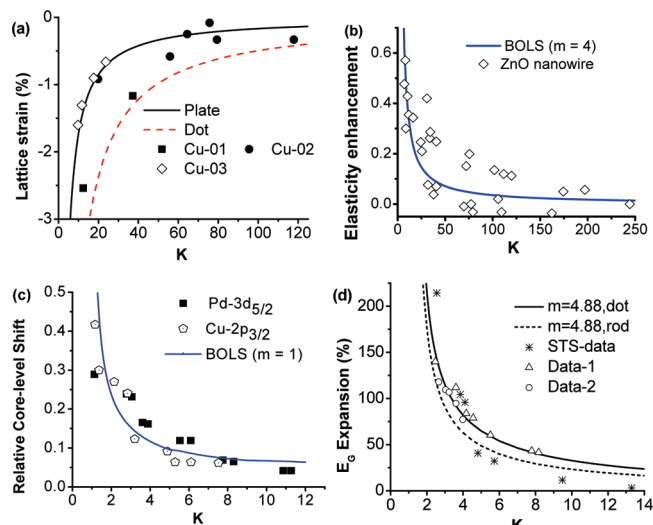
Coulomb Repulsion at the Nanometer-Sized Contact

J. Phys. Chem. C, Vol. 113, No. 46, 2009 **20015**

Figure 3. Comparison of theoretical predictions (solid lines) with the measured (scattered data) size dependence of (a) the Cu lattice strain;[91−93] (b) the elastic modulus (energy density) of ZnO nanowires;[94] (c) the core-level shift (potential trap depression) of Cu and Pd nanostructures;[71,95] and (d) band gap expansion of Si nanostructures measured using scanning tunnelling spectroscopy[64] and photoemission and photoabsorption method.[96,97]

of the surface local strain and skin-depth quantum trapping of charge and energy.

4.2. DFT Calculations. In order to further verify the concept of the broken-bond-induced charge and energy densification and quantum trapping, we choose the arm-chaired graphene nanoribbons (AGNR) and cuboctahedral (CO) gold atomic clusters of 13, 55, and 147 atoms for DFT calculations because the AGNR and Au cluster are ideal low-dimensional systems for concept verification. The DFT calculations were performed using the code DMOL3. All-electron calculations were performed with a double numeric plus polarization basis set. For the exchange and correlation term, the generalized gradient approximation was used as proposed by Perdew−Burke−Ernzerhof.[98] A finite basis-set cutoff was 4.1 Å, and self-consistent-field tolerance was 10^{-6} and 10^{-5} Hartree for GNR and Au. The forces and displacement in geometry optimizations were set respectively at 0.002 Hartree/Å and 0.005 Å. In order to test our method, we have calculated the DOS for perfect (10, 0) and (9, 0) CNTs. Our energy differences between the first two van Hove singularities are 0.82 eV for (10, 0) tube and 2.50 eV for (9, 0) tube, respectively. For Au clusters, calculations were focused on the coordination dependence of Au−Au bond length, the electron densities at the edge of gold nanoparticles.

Figure 4 shows the DFT calculation results on the width dependence of the (a) valence DOS and (b) the charge density per atom. As expected, an artificial band gap is generated for the AGNR. The upper branches in Figure 4a correspond to the polarized states and the lower ones to the trapped states. The separation between the two branches goes larger when the AGNR width becomes smaller. The DOS per atom in Figure 4a increases when the GNR width shrinks. The DOS of atoms in row 1, row 2, and row 3 are slightly different, showing the trend of edge significant. These findings are in good agreement with STM/S investigations, which confirmed the band gap expansion of Si nanowires[64] and the band gap generation of Au nanoparticles.[99] The calculated edge polarization also agrees with the STM/S observations that the extent of polarization and the density of charge are more pronounced at site closing to the edge.[72] These observations provide experimental
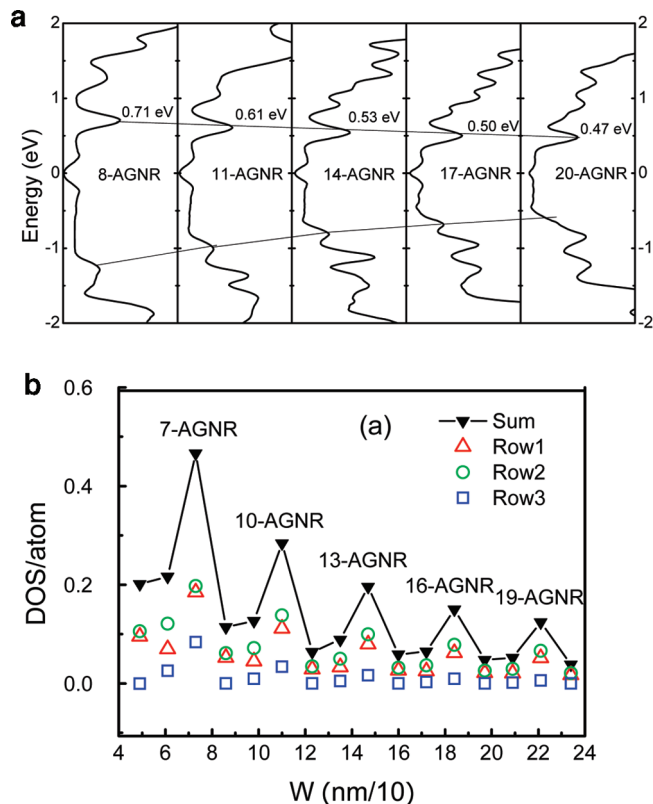

Figure 4. DFT computation results of the width dependent (edge-induced) (a) charge quantum trapping (<0) and polarization (>0) and (b) charge densification of the arm-chaired AGNR. Row 1, 2, and 3 is counted from the edge. Results verify the BOLS expectation of charge and energy quantum trapping and densification occurrences surrounding under-coordinated atoms at the edge.
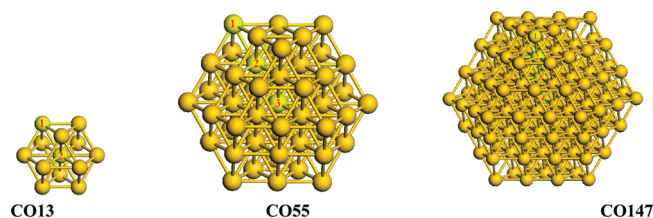

Figure 5. Structural configuration of the gold Cuboctahedral (CO) crystals of 13, 55, and 147 atoms with resolved corner, and the atomic layers.

and theoretical evidence for the BOLS predictions of the broken-bond-induced charge and energy quantum trapping and polarization and the associated charge densification.

Figure 5 shows the CO13, CO55, and CO147 structures of gold clusters. Calculation results show that the bonds between the less-coordinated atoms at corners or edges contract more significantly than those in the inner layer. The Au−Au distance contracts up to 20%, being in line with experimental observations of the Au cluster[12] and the BOLS expectation. Figure 6 shows the shell-resolved and the resultant valence DOS for the CO13, CO55, and CO147 clusters. It can be seen from panel a that the valence electrons in the outermost shell of the Co147 flows from deeper to the upper edge and the electrons in the inner shells shift insignificantly. The resultant DOS in panel b demonstrates the size dependence of charge polarization. The calculated trend agrees exceedingly well with experiment observations of the Au monatomic chain,[9] gold nanowires or islands on Au substradte,[10] silver monomer, dimer and quasi-dimer/monomer.[11] The common feature of these experimental observations is that the extent of polarization (energy and
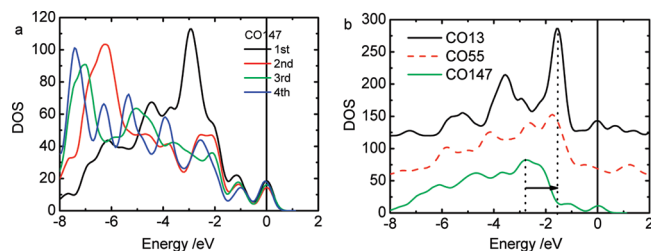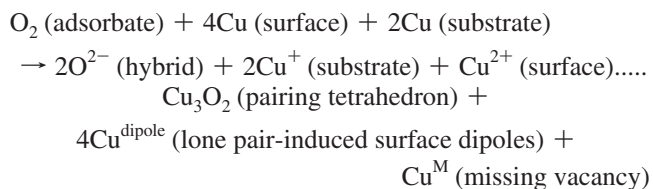
Figure 6. DFT derived (a) shell-resolved valence DOS and (b) the resultant DOS for the CO13, 55, 147 clusters. The former shows that the electrons of the least-coordinated atoms flow to the upper edge of the valence band and others shift slightly and the latter shows the trend of size dependence of charge polarization.

density) is more pronounced at sites of lower-coordinated atoms, which are in good accordance with the BOLS expectation and our DFT calculations.

4.3. STM and VLEED Confirmation. Some 10 years ago, we had conducted STM/S and VLEED analysis[7] of oxygen adsorption on Cu(001) surface. Here we present a brief summary on the key findings. Interested readers may be referred to a thematic report on oxidation electronics published in 2003[7] and a paper on nitriding electronics in 2006,[8] where we have analyzed a collection of STM/S, LEED, XPS, UPS, thermal desorption, and electron energy loss spectroscopy observations from more than 50 O-, N-, and C-induced surface phases with formulation of the atomic valence states and reaction dynamics.

Figure 7 shows the STM images of the clean Cu(001) (upper left) and the O−Cu-(001) surface with a scan difference of 0.045 nm[100] and the STS profiles (lower left) from clean Cu surface (curve A), on top (B), and side (C) of the O-induced protrusions.[101] The STS DOS at −2.0 eV corresponds to the lone pair state. The DOS annihilation around 0.5−2.0 eV arises from the occupation of the unoccupied DOS by the antibonding dipoles. The panel (lower right) is the bond model and the top and side views of the Cu(001) − ($\sqrt{2} \times 2\sqrt{2}$)R45° − 2O^{2-} complex unit cell with clear indication of the atomic valence of the individual atoms realized through the following processes of reaction[7]

$$O_2 \text{ (adsorbate)} + 4Cu \text{ (surface)} + 2Cu \text{ (substrate)}$$

$$\rightarrow 2O^{2-} \text{ (hybrid)} + 2Cu^+ \text{ (substrate)} + Cu^{2+} \text{ (surface).....}$$
$$Cu_3O_2 \text{ (pairing tetrahedron)} +$$

$$4Cu^{dipole} \text{ (lone pair-induced surface dipoles)} +$$

$$Cu^M \text{ (missing vacancy)}$$

VLEED is a technique that it is able to collect quantitative information from only the topmost two atomic layers regarding the bond geometry, charge density, surface potential-barrier height, and the bond forming kinetics under varied conditions. VLEED calculations revealed that the surface charge density of O−Cu(001) surface is 1.4 times that of a clean Cu(001) surface and that the origin of the surface potential-barrier shifts outward by 0.05 nm, being consistent with the STM topographic difference. The Cu$_3$O$_2$ forms in four-discrete stages and the Cu$_3$O$_2$ can be destroyed by heating at 500 °C. After several hours aging, the sp-orbit hybridization resumes. These STM/S and VLEED observations confirm the presence of lone pairs and the lone pair-induced dipoles at O−Cu surface.

4.4. XPS Verification of Defect States. In order to verify the enhancement of the quantum trapping and polarization, we conducted an *in situ* XPS measurement of SrTiO surface before

and after being sputtered by 3 keV Ar$^+$ beam for 20 min. The experiments were performed using the VG ESCALAB 220i-XL instrument (base pressure <5 × 10^{-10} mbar) with a monochromatic Al-K_α(1486.7 eV) X-ray source. All spectra were recorded in the constant pass energy mode with the pass energy set at 20 eV and step width of 0.1 eV. In this experiment, a SrTiO sample was first cleaned using an ultrasonic and put into the XPS chamber. After cooling down from annealing at 750 °C for one hour to the room temperature, the valence band and the O1s core level shift were detected. The cleanliness and chemical state of the substrate were ascertained by verifying the high-sensitivity and high-resolution XPS spectra measured. After 3 keV Ar$^+$ sputtering the measurement was repeated.

Figure 8 shows the XPS spectra collected from the smooth and Ar$^+$-roughened SrTiO surfaces. It is indeed very exciting that two additional DOS at 1 and 12 eV present in the valence band associated with a 0.6 eV positive shift of the O 1s core level energy. These findings confirm the BOLS expectation that Ar$^+$ sputtering roughens the surface with more defects around which atomic coordination is reduced. The additional DOS at 12 eV and the O1s shift arise from the defect-induced quantum trapping and the 1 eV DOS from the polarization. This experiment further confirms the BOLS expectation. Further investigation on the adatoms and surface defects induced quantum trapping and charge polarization is in progress.

4.5. Coulomb Repulsion at the Nanosized Contact Interface. We have thus far verified the skin-depth strain and quantum trapping of charge and energy both theoretically and experimentally and established the locked skin monopoles or dipoles in the counterparts of a nanosized liquid−solid or solid−solid contact. When two bodies of negative charges are placed together, interface Coulomb repulsion will be established, which lowers the contacting pressure and hence the frictional force. This process is independent of the drying or vacuum conditions or the applied pressure. However, if the applied pressure is too large compared with the Coulomb repulsion, the situation may change; kinetic energy dissipation takes place during sliding motion. If either side of the counterpart of friction is positively charged such as by H$^+$ termination[31] or hole (+) accumulation,[34] attraction force will be established and the friction will be enhanced.

The principle of fluid flow is that the bottom-most molecules of a liquid stick to the surface of the solid they are sliding past, creating friction that, for instance, slows down water flowing through a pipe. According to the BOLS correlation and current findings, the small fluidic drop can be viewed as a liquid core capped with a solidlike, densely charged, and elastic sheet with locked monopoles or dipoles at the surface. If the liquid−solid contacted counterparts are both negatively charged, charge sharing could not happen and the interface sticking could be thus prevented. The liquid droplet will react repulsively and elastically to the contacting body of which the surface is also negatively charged. If the droplet is sufficient small, the repulsion may levitate it, giving rise to superhydrophobicity. As can be seen from Figure 2, in the outermost two atomic layers of a smaller droplet, the energy density is even higher and the potential trap is even deeper, so that the effect of trapping and polarizing is even more apparent. The liquid drop and the channel wall surface are both negatively charged and they repel each other without being sticky to the counterparts. The droplet will lose its viscosity and becomes elastically frictionless. Such a system runs in a way more like a "magnetic levitation train" or a "hovercraft".
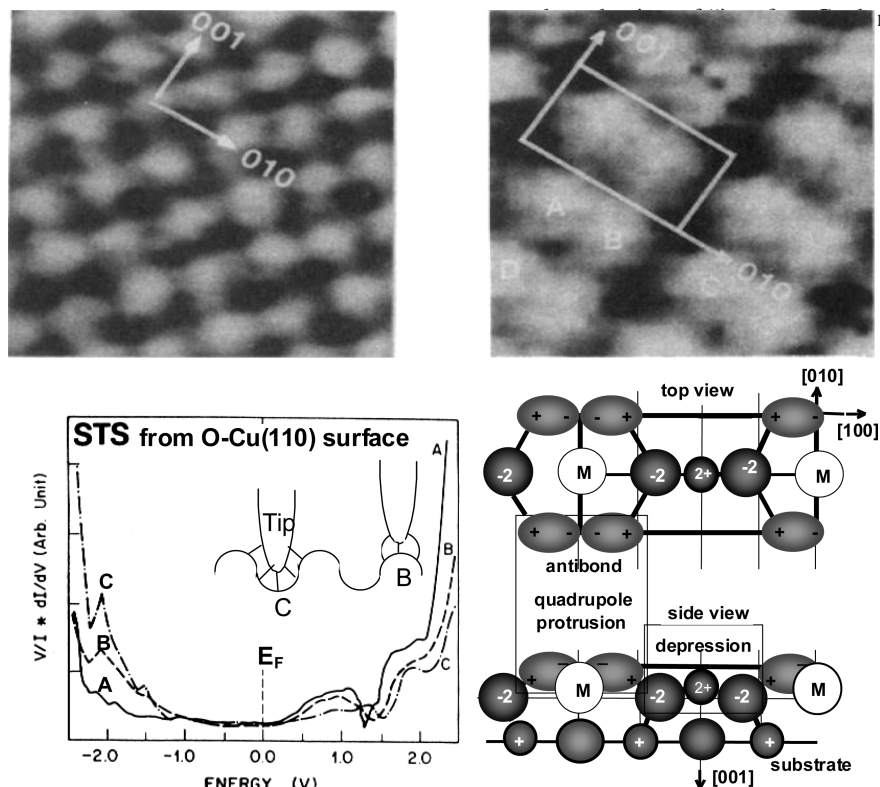
Coulomb Repulsion at the Nanometer-Sized Contact

J. Phys. Chem. C, Vol. 113, No. 46, 2009 **20017**

Figure 7. STM images of clean Cu(001) (upper left) and O−Cu-(001) surface with a scan difference of 0.045 nm[100] and the STS profiles (lower left) from clean Cu surface (curve A), on top (B), and side (C) of the O-induced protrusions. The STS DOS at −2.0 eV correspond to the lone pair and the DOS annihilation around 0.5−2.0 arises from the occupation of the unoccupied DOS by the antibonding dipoles. The panel (lower right) is the bond model and the top and side view of the Cu(001) − ($\sqrt{2} \times 2\sqrt{2}$)R45° − 2O^{2-} complex unit cell with clear indication of the atomic valence of the individual atoms realized through the processes of reaction as given in the text. VLEED calculations revealed that the surface charge density of O-added surface is 1.4 times that of the clean surface and the origin of potential barrier shift outward by 0.05 nm, being consistent with the STM topograph. These STM/S and VLEED observations confirm the presence of lone pairs and the lone pair-induced dipoles at O−Cu surface.

The mechanism of interface Coulomb repulsion also applies to the frictionless CNT linear bearing and the superlubricity of nanocontacts. Bond contraction happens to the multiwalled CNT causing elastic enhancement and charge densification. The unpaired π-electrons are further polarized, leading to the interwall repulsion and hence lower the friction. Bonds near the open ends of CNT contract even further, while the electrostatic force difference between the additionally densely charged CNT ends and the wall interior provides an additional force of the retraction of the CNTs to the mechanism proposed by Yuan and Zhao.[26] The water flow may induce additional charge at the open ends of CNTs.

The Coulomb repulsion between the "locked monopoles or dipoles in the stiffened skins" of the small grains could help in understanding the puzzle of ^{4}He crystal supersolidity in real space. The densification of energy corresponds to the enhancement of elasticity, which stiffens the solid skin allowing the ^{4}He segment to react elastically to a shear stress; the repulsion between the charged surfaces makes the frictionless motion. The extremely weak interatomic interaction between the He atoms makes the ^{4}He atoms or grains are nonsticky, more like hard spheres with close-filled electronic shells. The non-sticky interaction between grains will lower the friction coefficient. Lattice contraction of the supersolid ^{4}He segments is expected to happen, though this contraction may be too tiny[39] and needs to be verified experimentally.

5. Summary

In addition to the existing models from the perspectives of surface energetics and geometrical roughness, we proposed a
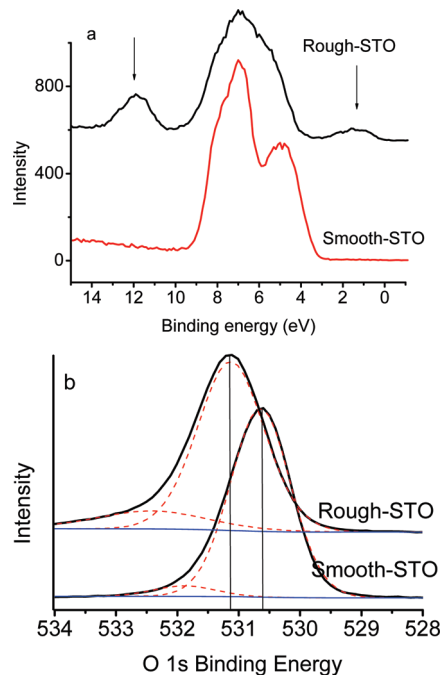

Figure 8. XPS spectra collected from the smooth and Ar$^+$-roughened SrTiO surfaces show (a) the presence of the additional valence DOS at 1 and 12 eV and (b) the O 1s core level shift of 0.6 eV. The additional DOS at 12 and 1 eV are attributed to the defect-induced trapping and polarization and the O1s energy shift confirms the defect-induced quantum trapping, being consistent with the results given in Figure 3c.

viewpoint of surface chemical nature to explain the historical puzzle of 4S. It is emphasized that the skin of a nanosized specimen is even more stiff with locked monopoles or dipoles and the extent of charge and energy densification is curvature dependent. Being similar to the "magnetic levitation", interface Coulomb repulsion due to the surface dipole formation upon F, O, or N addition or the presence of locked monopoles in the stiffened solid skins or the solidlike liquid skins dominates the 4S. This situation can be changed by removing the surface charge temporarily through UV irradiation, thermal excitation, excessive compressive stress, sputtering, or chemical doping to the sample. Understanding leads to clarification of the significance of broken bonds and nonbonding electrons in determining the nonsticky and frictionless motion in superhydrophobicity, superfluidity, superlubricity, and supersolidity at the nanometer sized contacts.

References and Notes

(1) Adam, N. K. *Nature* **1957**, *180*, 809.
(2) Cassie, A. B. D.; Baxter, S. *Trans. Faraday Soc.* **1944**, *40*, 546.
(3) Lafuma, A.; Quere, D. *Nat. Mater.* **2003**, *2*, 457.
(4) Gao, X. F.; Jiang, L. *Nature* **2004**, *432*, 36.
(5) Zheng, Q. S.; Yu, Y.; Feng, X. Q. *J. Adhes. Sci. Technol.* **2009**, *23*, 493.
(6) Sun, C. Q. *Prog. Solid State Chem.* **2007**, *35*, 1.
(7) Sun, C. Q. *Prog. Mater Sci.* **2003**, *48*, 521.
(8) Zheng, W. T.; Sun, C. Q. *Prog. Solid State Chem.* **2006**, *34*, 1.
(9) Crain, J. N.; Pierce, D. T. *Science* **2005**, *307*, 703.
(10) Schouteden, K.; Lijnen, E.; Muzychenko, D. A.; Ceulemans, A.; Chibotaru, L. F.; Lievens, P.; Haesendonck, C. V. *Nanotechnology* **2009**, *20*, 395401.
(11) Sperl, A.; Kroger, J.; Berndt, R.; Franke, A.; Pehlke, E. *New J. Phys.* **2009**, *11*, 063020.
(12) Huang, W. J.; Sun, R.; Tao, J.; Menard, L. D.; Nuzzo, R. G.; Zuo, J. M. *Nat. Mater.* **2008**, *7*, 308.
(13) Li, W.; Amirfazli, A. *Adv. Mater.* **2007**, *19*, 3421.
(14) Li, X. M.; Reinhoudt, D.; Crego-Calama, M. *Chem. Soc. Rev.* **2007**, *36*, 1350.
(15) Lee, C.; Choi, C. H.; Kim, C. J. *Phys. Rev. Lett.* **2008**, *101*, 064501.
(16) Fang, G. P.; Li, W.; Wang, X. F.; Qiao, G. J. *Langmuir* **2008**, *24*, 11651.
(17) Li, W.; Fang, G. P.; Lij, Y. F.; Qiao, G. J. *J. Phys. Chem. B* **2008**, *112*, 7234.
(18) Zheng, X. P.; Zhao, H. P.; Gao, L. T.; Liu, J. L.; Yu, S. W.; Feng, X. Q. *J. Colloid Interface Sci.* **2008**, *323*, 133.
(19) Caputo, G.; Cingolani, R.; Cozzoli, P. D.; Athanassiou, A. *Phys. Chem. Chem. Phys.* **2009**, *11*, 3692.
(20) Sun, R. D.; Nakajima, A.; Fujishima, A.; Watanabe, T.; Hashimoto, K. *J. Phys. Chem. B* **2001**, *105*, 1984.
(21) Schoch, R. B.; Han, J. Y.; Renaud, P. *Rev. Mod. Phys.* **2008**, *80*, 839.
(22) Wong, K. F. V.; Kurma, T. *Nanotechnology* **2008**, *19*, 345702.
(23) Thomas, J. A.; McGaughey, A. J. H. *Nano Lett.* **2008**, *8*, 2788.
(24) Whitby, M.; Cagnon, L.; Thanou, M.; Quirke, N. *Nano Lett.* **2008**, *8*, 2632.
(25) Majumder, M.; Chopra, N.; Andrews, R.; Hinds, B. J. *Nature* **2005**, *438*, 44.
(26) Yuan, Q. Z.; Zhao, Y. P. *J. Am. Chem. Soc.* **2009**, *131*, 6374.
(27) Baldessari, F. *J. Colloid Interface Sci.* **2008**, *325*, 526.
(28) Socoliuc, A.; Gnecco, E.; Maier, S.; Pfeiffer, O.; Baratoff, A.; Bennewitz, R.; Meyer, E. *Science* **2006**, *313*, 207.
(29) Gnecco, E.; Maier, S.; Meyer, E. *J. Phys.: Condens. Matter* **2008**, *20*, 354004.
(30) Cumings, J.; Zettl, A. *Science* **2000**, *289*, 602.
(31) Cannara, R. J.; Brukman, M. J.; Cimatu, K.; Sumant, A. V.; Baldelli, S.; Carpick, R. W. *Science* **2007**, *318*, 780.
(32) Socoliuc, A.; Bennewitz, R.; Gnecco, E.; Meyer, E *Phys. Rev. Lett.* **2004**, *92*, 134301.
(33) *Superlubricity*; Erdemir, A., Martin, J. M., Eds.; Elsevier: New York, 2007.
(34) Park, J. Y.; Ogletree, D. F.; Thiel, P. A.; Salmeron, M. *Science* **2006**, *313*, 186.
(35) Tomlinson, G. A. *Philos. Mag.* **1929**, *7*, 905.
(36) Prandtl, L. *Z. Angew. Math. Mech.* **1928**, *8*, 85.
(37) Mo, Y. F.; Turner, K. T.; Szlufarska, I. *Nature* **2009**, *457*, 1116.
(38) Kim, E.; Chan, M. H. W. *Nature* **2004**, *427*, 225.
(39) Balibar, S.; Caupin, F. *J. Phys.: Condens. Matter* **2008**, *20*, 173201.
(40) Hunt, B.; Pratt, E.; Gadagkar, V.; Yamashita, M.; Balatsky, A. V.; Davis, J. C. *Science* **2009**, *324*, 632.
(41) Day, J.; Beamish, J. *Nature* **2007**, *450*, 853.
(42) Anderson, P. W. *Science* **2009**, *324*, 631.
(43) Pollet, L.; Boninsegni, M.; Kuklov, A. B.; Prokof'ev, N. V.; Svistunov, B. V.; Troyer, M. *Phys. Rev. Lett.* **2008**, *101*, 097202.
(44) Sasaki, S.; Ishiguro, R.; Caupin, F.; Maris, H. J.; Balibar, S. *Science* **2006**, *313*, 1098.
(45) Saunders, J. *Science* **2009**, *324*, 601.
(46) Matsui, F.; Matsushita, T.; Kato, Y.; Hashimoto, M.; Inaji, K.; Guo, F. Z.; Daimon, H. *Phys. Rev. Lett.* **2008**, *100*, 207201.
(47) Sun, C. Q. *Phys. Rev. B* **2004**, *69*, 045105.
(48) Pershan, P. S.; Stoltz, S. E.; Shpyrko, O. G.; Deutsch, M.; Balagurusamy, V. S. K.; Meron, M.; Lin, B.; Streitel, R. *Phys. Rev. B* **2009**, *79*, 115417.
(49) Shpyrko, O. G.; Grigoriev, A. Y.; Steimer, C.; Pershan, P. S.; Lin, B. H.; Meron, M.; Graber, T.; Gerbhardt, J.; Ocko, B.; Deutsch, M. *Phys. Rev. B* **2004**, *70*, 224206.
(50) Tsai, Y. C.; Hsu, C. W.; Yu, J. S. K.; Lee, G. H.; Wang, Y.; Kuo, T. S. *Angew. Chem., Int. Ed.* **2008**, *47*, 7250.
(51) Noor, A.; Wagner, F. R.; Kempe, R. *Angew. Chem., Int. Ed.* **2008**, *47*, 7246.
(52) Untiedt, C.; Yanson, A. I.; Grande, R.; Rubio-Bollinger, G.; Agrait, N.; Vieira, S.; van Ruitenbeek, J. M. *Phys. Rev. B* **2002**, *66*, 085418.
(53) Smit, R. H. M.; Untiedt, C.; Yanson, A. I.; van Ruitenbeek, J. M. *Phys. Rev. Lett.* **2001**, *87*, 266102.
(54) Kizuka, T. *Phys. Rev. B* **2008**, *77*, 155401.
(55) Sun, C. Q.; Bai, H. L.; Tay, B. K.; Li, S.; Jiang, E. Y. *J. Phys. Chem. B* **2003**, *107*, 7544.
(56) Sun, C. Q.; Fu, S. Y.; Nie, Y. G. *J. Phys. Chem. C* **2008**, *112*, 18927.
(57) Rastei, M. V.; Heinrich, B.; Limot, L.; Ignatiev, P. A.; Stepanyuk, V. S.; Bruno, P.; Bucher, J. P. *Phys. Rev. Lett.* **2007**, *99*, 246102.
(58) Mironets, O.; Meyerheim, H. L.; Tusche, C.; Stepanyuk, V. S.; Soyka, E.; Zschack, P.; Hong, H.; Jeutter, N.; Felici, R.; Kirschner, J. *Phys. Rev. Lett.* **2008**, *100*.
(59) Qi, W. H.; Huang, B. Y.; Wang, M. P. *Nanoscale Res. Lett.* **2009**, *4*, 269.
(60) Qi, W. H.; Huang, B. Y.; Wang, M. P. *J. Adhes. Sci. Technol.* **2009**, *6*, 635.
(61) Ding, Y.; Sun, C. Q.; Zhou, Y. C. *J. Appl. Phys.* **2008**, *103*, 084317.
(62) Liu, X. J.; Li, J. W.; Zhou, Z. F.; Yang, L. W.; Ma, Z. S.; Xie, G. F.; Pan, Y.; Sun, C. Q. *Appl. Phys. Lett.* **2009**, *94*, 131902.
(63) Roduner, E. *Chem. Soc. Rev.* **2006**, *35*, 583.
(64) Ma, D. D. D.; Lee, C. S.; Au, F. C. K.; Tong, S. Y.; Lee, S. T. *Science* **2003**, *299*, 1874.
(65) Fang, B. S.; Lo, W. S.; Chien, T. S.; Leung, T. C.; Lue, C. Y.; Chan, C. T.; Ho, K. M. *Phys. Rev. B* **1994**, *50*, 11093.
(66) Bartynski, R. A.; Heskett, D.; Garrison, K.; Watson, G.; Zehner, D. M.; Mei, W. N.; Tong, S. Y.; Pan, X. *J. Vac. Sci. Technol., A* **1989**, *7*, 1931.
(67) Kim, K. J.; Lee, H.; Choi, J. H.; Youn, Y. S.; Choi, J.; Kang, T. H.; Jung, M. C.; Shin, H. J.; Lee, H. J.; Kim, S.; Kim, B. *Adv. Mater.* **2008**, *20*, 3589.
(68) Hibino, H.; Kageshima, H.; Kotsugi, M.; Maeda, F.; Guo, F.-Z.; Watanabe, Y. *Phys Rev B* **2009**, *79*, 125431.
(69) Sun, C. Q.; Tay, B. K.; Lau, S. P.; Sun, X. W.; Zeng, X. T.; Li, S.; Bai, H. L.; Liu, H.; Liu, Z. H.; Jiang, E. Y. *J. Appl. Phys.* **2001**, *90*, 2615.
(70) Sun, C. Q. *Prog. Mater Sci.* **2009**, *54*, 179.
(71) Rao, C. N. R.; Kulkarni, G. U.; Thomas, P. J.; Edwards, P. P. *Chem.—Eur. J.* **2002**, *8*, 29.
(72) Niimi, Y.; Matsui, T.; Kambara, H.; Fukuyama, H. *Phys. E* **2005**, *34*, 100.
(73) Crain, J. N.; Stiles, M. D.; Stroscio, J. A.; Pierce, D. T. *Phys. Rev. Lett.* **2006**, *96*, 156801.

(74) Nakada, K.; Fujita, M.; Dresselhaus, G.; Dresselhaus, M. S. *Phys. Rev. B* **1996**, *54*, 17954.

(75) Pinto, R. A.; Haque, M.; Flach, S. *Phys. Rev. A* **2009**, *79*, 052118.

(76) Matsuda, I.; Liu, C.; Hirahara, T.; Ueno, M.; Tanikawa, T.; Kanagawa, T.; Hobara, R.; Yamazaki, S.; Hasegawa, S. *Phys. Rev. Lett.* **2007**, *99*, 146805.

(77) Schiller, F.; Heber, M.; Servedio, V. D. P.; Laubschat, C. *Phys. Rev. B* **2004**, *70*, 125106.

(78) Wang, B.; Xiao, X. D.; Huang, X. X.; Sheng, P.; Hou, J. G. *Appl. Phys. Lett.* **2000**, *77*, 1179.

(79) Hou, J. G.; Wang, B.; Yang, J. L.; Wang, X. R.; Wang, H. Q.; Zhu, Q. S.; Xiao, X. D. *Phys. Rev. Lett.* **2001**, *86*, 5321.

(80) Liu, X.; Bauer, M.; Bertagnolli, H.; Roduner, E.; van Slageren, J.; Phillipp, F. *Phys. Rev. Lett.* **2006**, *97*, 253401.

(81) Coey, J. M. D. *Curr. Opin. Solid State Mater. Sci.* **2006**, *10*, 83.

(82) Street, R. A. *Hydrogenated amorphous silicon*; Cambridge University Press: New York, 1991.

(83) Abbas, Z.; Labbez, C.; Nordholm, S.; Ahlberg, E. *J. Phys. Chem. C* **2008**, *112*, 5715.

(84) Liu, D.; Lian, J. S.; Jiang, Q. *J. Chem. Phys. C* **2009**, *113*, 1168.

(85) Pabisiak, T.; Kiejna, A. *Phys. Rev. B* **2009**, *79*, 10.

(86) Magnusson, M. H.; Deppert, K.; Malm, J. O.; Bovin, J. O.; Samuelson, L. *J. Nanopart. Res.* **1999**, *1*, 243.

(87) Nasibulin, A. G.; Shandakov, S. D.; Anisimov, A. S.; Gonzalez, D.; Jiang, H.; Pudas, M.; Queipo, P.; Kauppinen, E. I. *J. Chem. Phys. C* **2008**, *112*, 5762.

(88) Leung, C.; Kinns, H.; Hoogenboom, B. W.; Howorka, S.; Mesquida, P. *Nano Lett.* **2009**, *9*, 2769.

(89) Jakubczyk, D.; Kolwas, M.; Derkachov, G.; Kolwas, K. *J. Phys. Chem. C* **2009**, *113*, 10598.

(90) Liu, S.; Luo, J.; Xie, G.; Guo, D. *J. Appl. Phys.* **2009**, *105*, 124301.

(91) Apai, G.; Hamilton, J. F.; Stohr, J.; Thompson, A. *Phys. Rev. Lett.* **1979**, *43*, 165.

(92) Wasserma, H. J.; Vermaak, J. S. *Surf. Sci.* **1972**, *32*, 168.

(93) Kara, A.; Rahman, T. S. *Phys. Rev. Lett.* **1998**, *81*, 1453.

(94) Chen, C. Q.; Shi, Y.; Zhang, Y. S.; Zhu, J.; Yan, Y. J. *Phys. Rev. Lett.* **2006**, *96*, 075505.

(95) Yang, D. Q.; Sacher, E. *Appl. Surf. Sci.* **2002**, *195*, 187.

(96) Pan, L. K.; Sun, C. Q.; Tay, B. K.; Chen, T. P.; Li, S. *J. Phys. Chem. B* **2002**, *106*, 11725.

(97) Campbell, I. H.; Fauchet, P. M. *Solid State Commun.* **1986**, *58*, 739.

(98) Perdew, J. P.; Burke, K.; Ernzerhof, M. *Phys. Rev. Lett.* **1996**, *77*, 3865.

(99) Wang, B.; Wang, K. D.; Lu, W.; Yang, J. L.; Hou, J. G. *Phys. Rev. B* **2004**, *70*, 205411.

(100) Jensen, F.; Besenbacher, F.; Laegsgaard, E.; Stensgaard, I. *Phys. Rev. B* **1990**, *42*, 9206.

(101) Chua, F. M.; Kuk, Y.; Silverman, P. J. *Phys. Rev. Lett.* **1989**, *63*, 386.